Heterogenous contribution of the Southern Ocean to deglacial atmospheric CO_2 rise

Andrew D. Moy[1,2*], Martin R. Palmer[3], William R. Howard[4], Jelle Bijma[5], Matthew J. Cooper[3], Eva Calvo[6], Carles Pelejero[6,7], Michael K. Gagan[8,9], Thomas B. Chalk[3]

[1] Australian Antarctic Division, 203 Channel Highway, Kingston, Tasmania 7050, Australia

[2] Antarctic Climate and Ecosystems Cooperative Research Centre, University of Tasmania, Hobart, Tasmania 7000, Australia

[3] Ocean and Earth Science, University of Southampton, European Way, Southampton, SO14 3ZH, UK

[4] Climate Change Institute, The Australian National University, Canberra, Australian Capital Territory 2601, Australia

[5] Marine Biogeosciences, Alfred-Wegener-Institut Helmholtz-Zentrum für Polar- und Meeresforschung, Am Handelshafen 12, 27570 Bremerhaven, Germany

[6] ICM-CSIC, Institut de Ciències del Mar, Passeig Marítim de la Barceloneta 37-49, 08003 Barcelona, Catalunya, Spain

[7] ICREA, Institució Catalana de Recerca i Estudis Avançats, Passeig Lluís Companys 23, 08010 Barcelona, Catalunya, Spain

[8] Research School of Earth Sciences, The Australian National University, Acton, Australian Capital Territory 2601, Australia

[9] School of Earth and Environmental Sciences, The University of Queensland, Brisbane, Queensland 4072, Australia

*e-mail: Andrew.Moy@aad.gov.au

Glacial-interglacial changes in atmospheric CO_2 are generally attributed to changes in ocean carbon chemistry in response to large-scale shifts in the ocean's biology, alkalinity and physical circulation. The modern ocean plays an important role in regulating CO_2, with the Southern Ocean taking up more CO_2 than any other. It is likely to have played a crucial role in controlling past atmospheric CO_2. However, the physical, biological and chemical variables involved in controlling ocean-atmosphere CO_2 exchange during glacial-interglacial cycle are not completely understood. Here we use boron isotopes, carbon isotopes in planktonic foraminifera and an alkenone-based proxy of temperature to reconstruct seawater pH and CO_2 partial pressure in sub-Antarctic surface waters, and investigate the mechanisms regulating surface water CO_2 over the last glacial-interglacial cycle. Our reconstruction over the last 25,000 years, from a sediment core recovered south of Tasmania, shows surface waters in that region were a sink for atmospheric CO_2 during the Last Glacial Maximum. Our reconstruction suggests changes in the strength of the biological pump and the release of deep-ocean CO_2 to surface waters contributed to the last deglacial atmospheric CO_2 rise. These findings demonstrate that variations in the distribution of Southern Ocean water masses in this sector and upwelling intensity played a key role in regulating atmospheric CO_2 during the last glacial-interglacial cycle.

Atmospheric CO_2 concentrations range from minima of ~180 ppmv during glacial intervals to maxima of ~280-300 ppmv during interglacial intervals[1]. The ocean is the largest active carbon reservoir; hence, changes in ocean-atmosphere interactions, ocean circulation and marine biogeochemistry likely played major roles in modulating glacial-interglacial (G-IG) atmospheric CO_2 variability[2-5]. Despite this understanding of the ocean's overall role in modulating atmospheric CO_2, information on the time and spatial evolution of ocean source-sink behaviour remains scarce. Determining the factors controlling ocean-atmosphere CO_2

dynamics requires an understanding of the natural physical and biological processes that affect the state of CO_2 in ocean, and this is of key importance in validating the different mechanisms used in geochemical models to explain G-IG variations in atmospheric CO_2 (e.g. refs 6-10). Changes in these processes in the Southern Ocean are hypothesised to have been crucial[10-19], however, direct proxy histories of variables reflecting past G-IG changes in surface-ocean pCO_2 are limited to one record of deglacial change in the Atlantic sector of the Southern Ocean[15] that only captures part of the G-IG change in atmospheric CO_2. Our study focuses on the Indo-Pacific sector of the Southern Ocean south of Australia and, for the first time, we present a Southern Ocean surface-ocean carbonate chemistry reconstruction that allows the quantification of ocean-atmosphere CO_2 exchange accompanying the full G-IG rise in atmospheric CO_2.

We analysed $\delta^{18}O$, $\delta^{13}C$, $\delta^{11}B$, and shell weight for the planktonic foraminifer *Globigerina bulloides* in sediment core MD972106 (45°09'S, 146°17'E, water depth 3310 m; see Methods) to reconstruct surface water pH and CO_2 partial pressure (pCO_2) over the last 25 kyr (thousand years) in the Southern Ocean region south of Tasmania. Long-term climatological studies[20] show that the core site is located at the southern edge of the Subtropical Front (STF), that marks the northern boundary of the Southern Ocean separating the Subtropical Zone (STZ) from the sub-Antarctic Zone (SAZ) surface waters, and is bathed by Lower Circumpolar Deep Water (Fig. 1 and Supplementary Fig. 1). The core site is also located just north (defined by the STF) of the high nutrient, low chlorophyll (HNLC) area of the Southern Ocean[21]. Sea-surface temperature (SST) reconstructions for the Late Quaternary indicate that the STF migrated north of its present position during glacial periods and was at its most northerly position at the last glaciation[22]. Thus we infer surface waters over MD972106 during the last glaciation had SAZ properties.

Glacial-interglacial palaeo-proxy record

Down-core variations in *G. bulloides* $\delta^{18}O$ exhibit a G-IG amplitude of ~2 ‰ (Fig. 2a). The G-IG change in global ocean $\delta^{18}O$ is estimated to have been ~1.1 ‰ (ref. 23), hence the ~2 ‰ shift in the *G. bulloides* $\delta^{18}O$ record requires a SST (and a carbonate ion effect[24]) component, which is quantified here using alkenone derived SSTs. The Holocene and Last Glacial Maximum (LGM, ~18 to 22 ka, thousand years ago) $\delta^{13}C$ averages are similar, but the G-IG transition displays a minimum at ~12 ka, and a minimum during the Holocene at ~7.4 ka (Fig. 2b). *Globigerina bulloides* shell weights are heavier during glacial times (Fig. 2c). There is also a clear difference in *G. bulloides* $\delta^{11}B$ values, with Holocene $\delta^{11}B$ about 2.0 ‰ lower than in the LGM (Fig. 2d). Alkenone-based SST estimates show a G-IG change of ~4.1°C with a minimum of 8.2°C at ~21.4 ka, followed by post-glacial warming to 13.9°C at ~11 kyr and cooling to ~13°C over the past ~6 kyr (Fig. 2e). The most recent samples (~2.6 to 2 ka) show deviations in $\delta^{18}O$, shell weight and $\delta^{11}B$ compared to earlier Holocene values. The $\delta^{18}O$ and shell weights are confirmed with replicate sample measurements.

Down-core *G. bulloides* $\delta^{18}O$, $\delta^{11}B$ and shell weights co-vary with each other (Fig. 2) and with atmospheric CO_2 over the last 25 kyr (Fig. 3b). This co-variation is interpreted here to arise from G-IG evolution of surface water temperature and chemistry[24-29]. Because MD972106 was recovered at a depth above and close to the modern calcite saturation horizon (Supplementary Fig. 2), it is important to consider the possible effects of post-depositional calcite dissolution on shell weights[28,30], particularly when considering G-IG lysocline changes versus primary calcification driven by surface water carbonate ion concentration ($[CO_3^{2-}]$). Holocene core-top *G. bulloides* shell weights indicate the foraminiferal lysocline at the South Tasman Rise is at ~3,600m water depth[31]. Carbonate preservation indicators, percent calcium carbonate and percent whole foraminifera (Supplementary Fig. 3), suggest that calcite dissolution did not play a significant role over the past 25 kyr at this site.

Reconstructing seawater pH and pCO_2

Past variations in sea surface water pH at the site of MD972106 are calculated from the δ^{11}B-pH relationship for *G. bulloides*[32] and the alkenone SST record (see Methods). Estimated pH shows a decline from LGM values of ~8.38 to Holocene values of ~8.16 (Fig. 3a). By comparison, the modern anthropogenic-influenced surface water pH value at the MD972106 site was 8.11 in 2001 (Supplementary Note 1). Variations in surface water pCO_2 (Fig. 3b) over the past 25 kyr can be estimated using the SST alkenone record, the δ^{11}B surface water pH record and estimates of either alkalinity or DIC (see Methods). There is close agreement between pCO_2 calculated using estimates of pH combined with either; (1) estimates of alkalinity or (2) DIC (Fig. 3b). Methods (1) and (2) both use pH estimated from *G. bulloides* δ^{11}B, and hence any differences result from the assumptions underlying estimates of the alkalinity and DIC parameters, respectively. These calculations show surface water pCO_2 rising from ~165 ppmv at the LGM to ~280 ppmv in the early Holocene (Fig. 3b). The interval ~6.3 to 4.2 ka is marked by elevated pCO_2 of ~315 to 360 ppmv that decreases to ~270 ppmv at ~2 ka (Fig. 3b). The 2001 surface water pCO_2 at this site was ~330 ppmv, broadly consistent with the known anthropogenic rise in atmospheric CO_2 (Supplementary Note 1).

The difference between the pCO_2 value of the surface water and atmosphere (ΔpCO_2) can be calculated by comparison with ice core CO_2 data from Antarctica[33] (Fig. 3b). Estimated ΔpCO_2 (Fig. 3c, 5e) indicates that surface waters near MD972106 were a net sink for atmospheric CO_2 during the LGM (ΔpCO_2 = -25 ppmv) and continued to operate in this way during the G-IG transition until ~12 ka, where surface waters became a net source of CO_2 during the early Holocene (ΔpCO_2 = 15 ppmv). Between ~6.3 to 4.2 ka the surface waters were a strong net source for atmospheric CO_2 (ΔpCO_2 ~50 to 90 ppmv), before becoming again a weak net sink (ΔpCO_2 ~ -6 ppmv) at ~2 ka (Fig. 3c, 5e). In addition, past surface seawater

[CO_3^{2-}] calculated from estimates of pH, SST and alkalinity (and DIC) show surface water [CO_3^{2-}] falling from ~265 μmol kg^{-1} in the LGM to ~190 μmol kg^{-1} for most of the Holocene (Fig. 4a). The anthropogenically perturbed surface water [CO_3^{2-}] at this site is ~183 μmol kg^{-1} whereas the pre-industrial [CO_3^{2-}] is estimated to be ~212 μmol kg^{-1} (Supplementary Note 2), which is within the uncertainty of the most recent Holocene [CO_3^{2-}] (Fig. 4a).

The shell weight-[CO_3^{2-}] relationship[27] was also applied to the MD972106 data to reconstruct [CO_3^{2-}] for surface waters over the past 25 kyr (Fig. 4b). The close agreement between estimated surface water [CO_3^{2-}] derived from these two independent proxies (*G. bulloides* $\delta^{11}B$ values and shell weight) reinforces our findings that $\delta^{11}B$ of *G. bulloides* yields reliable reconstructions of seawater pH.

Southern Ocean contribution to atmospheric CO_2 change

Our reconstruction is consistent with the hypothesis that the G-IG modulation of the Southern Ocean carbon sink likely arose from changes in SST, biogeochemistry and ocean circulation, specifically; 1) colder LGM seawater increased CO_2 solubility; 2) a stronger 'biological pump' during the LGM reduced the DIC in surface waters; and 3) surface water pH and carbonate ion concentration [CO_3^{2-}] was higher during the LGM.

Two hypotheses involving the Southern Ocean have been offered to explain G-IG cycles in atmospheric CO_2. The first invokes increased strength of the biological (or 'soft-tissue') pump in the high-latitude Southern Ocean during the LGM[6-8,11] in response to an increase in nutrient utilisation, possibly through iron fertilisation[34], in sub-Antarctic surface waters. This is supported by studies indicating that export production in the area between the STF and PF were higher during the LGM than the Holocene[14,35-37]. The second invokes decreased exchange between surface waters and the deep-ocean south of the Polar Front[38-40]. The increased stratification reduces upwelling and exchange of nutrient and CO_2 rich deep-

waters with the surface ocean. This is supported by increased nutrient utilisation as shown by $\delta^{15}N$ records[38], reduced ventilation of the deep Southern Ocean[41], and subsequent increase in ocean CO_2 storage[17,19] during the LGM. No single mechanism[42] can explain the full glacial draw-down in atmospheric CO_2, although a combination of mechanisms has been proposed[2,14,16].

Zonal Asymmetry of deglacial change in the Southern Ocean

Our full deglacial Southern Ocean pH and pCO_2 reconstruction can be compared to a reconstruction of late deglacial pH and pCO_2 in the Atlantic sector of the subantarctic Southern Ocean[15], to provide further insights into the subantarctic role in CO_2 change. A reconstruction of surface ocean pCO_2, spanning ~16-2 kyr and also utilising $\delta^{11}B$ and $\delta^{13}C$ of *G. bulloides*[15] was undertaken at a site in the Atlantic-sector SAZ at a similar latitude to MD972106. That study, while not spanning the full deglacial amplitude of CO_2 change, suggested surface waters in that sector were in approximate equilibrium with the atmosphere at ~16 ka and became a strong net source of CO_2 to the atmosphere (ΔpCO_2 of ~50 ppmv; Fig. 5e) by ~15 ka, before declining intermittently to reach approximate atmospheric equilibrium at ~4 ka. That pattern was interpreted to suggest that there was enhanced upwelling of deep waters in the Atlantic sector of the SAZ during the deglaciation.

At our site south of Tasmania, surface waters were a net sink for atmospheric CO_2 (ΔpCO_2 = -25 ppmv) during the LGM (Fig. 3c, 5e). The northward migration of the STF at the LGM[22] resulted in an expansion of the Southern Ocean water masses, and coincided with increased delivery of bioavailable dust-borne iron to the ocean[34]; both of these processes would also lead to the expansion of the zone of high biological production in the Southern Ocean. At the same time, the stratification of the deep Southern Ocean during the LGM reduced the contribution of upwelling of more dissolved CO_2 to surface waters. At the site of MD972106,

G. bulloides $\delta^{13}C$ temperature- and $[CO_3^{2-}]$-adjusted ($\delta^{13}C_{adj}$) values (see Methods for details on these adjustments), and the $\delta^{13}C$ gradient between planktonic and benthic foraminifera ($\Delta\delta^{13}C$ gradient) were largest during the LGM (Fig. 5a, c), indicating high primary productivity[43,44]. Similarly, alkenone concentrations (Fig. 5d) were highest during the LGM and provide qualitative information on past productivity of coccolithophorid algae[45,46]. Comparison of alkenone concentrations (Fig. 5d.) and ΔpCO_2 (Fig. 5e.) shows that, when there was maximum biological production in this region, CO_2 degassing was suppressed. Our data suggests the biological pump was stronger during the LGM (i.e. the DIC gradient between surface and deep ocean increased), possibly through iron fertilisation[34,47], and steadily decreased over the last deglaciation. Changes in the strength of the biological pump could also be related to changes in circulation[48], via a more isolated deep ocean, in particular south of the Polar Front[38].

The $\delta^{13}C$ recorded by *G. bulloides* in the Atlantic sector of the SAZ shows a ~1.5 ‰ decrease from the LGM to the onset of maximum CO_2 degassing (not shown)[15], while the MD972106 site shows a smaller decrease ($\delta^{13}C$ decrease of ~0.3 ‰, Fig. 2b; $\delta^{13}C_{adj}$ decrease of ~0.1 ‰, Fig. 5a) over the same period. The inferred increase in upwelling in the Atlantic sector is not reflected in the reconstructed ΔpCO_2 record at MD972106 (Fig. 3c, 5e). Surface waters at MD972106 during the last deglaciation remained a net sink for CO_2 (average ΔpCO_2 = -25 ppmv; Fig. 3c, 5e). The steadily decreasing $\delta^{13}C_{adj}$ (Fig. 5a) and $\Delta\delta^{13}C$ gradient (Fig. 5c) during the last deglaciation is consistent with a progressive increase in the contribution of upwelling and advection of 'old' CO_2-rich (and ^{13}C-depleted water) CDW to sub-Antarctic surface waters. Nevertheless, surface waters remained a net sink for atmospheric CO_2 during this period, suggesting that productivity (drawdown of CO_2) likely kept in pace with any augmented nutrient supply, and compensated for any increased CO_2 from upwelling in this

subantarctic region. Alkenone concentrations (a proxy for coccolithophorid algae primary/export production; Fig. 5d) shows enhanced biological productivity was maintained during this interval. There is compelling evidence for a build-up of carbon in the deep Southern Ocean towards the LGM[12,17,19], and subsequent release and ventilation[41] of this deep carbon store during the last deglaciation which is consistent with the rise in atmospheric CO_2 (refs 17, 19).

The interval between ~6.3 to 4.2 ka, when surface waters at MD972106 were a net source of atmospheric CO_2 (ΔpCO_2 of ~50 to 90 ppmv; Fig. 3c, 5e), coincides with a period of strengthened Southern Hemisphere Westerly Winds (SWW) inferred from analysis of terrestrial records[49,50]. Changes in the latitude and intensity of the SWW are potential drivers of changes in atmospheric CO_2, as suggested by modelling[10], opal burial rates[51] and is with agreement of equatorial and Antarctic carbon isotope variations[52]. Intensification of SWW increases the contribution of upwelled CO_2-rich CDW (and low $\delta^{13}C$ water) to surface waters within the Antarctic Zone. *G. bulloides* $\delta^{13}C_{adj}$ at MD972106 reach a minimum at ~7.4 ka (Fig. 5a) and $\Delta\delta^{13}C$ gradient falls below the Holocene average gradient (Fig. 5c). Our data are thus consistent with the hypothesis that the net CO_2 source during this period resulted from increased upwelling of CO_2-rich CDW within the Antarctic Zone that advected northward to SAZ surface waters by the strengthened SWW[49,50].

The deviations in the most recent *G. bulloides* samples ($\delta^{18}O$, shell weight and $\delta^{11}B$; Fig 2.) stand in contrast to earlier Holocene values, and reflects changing surface water CO_2 dynamics. Surface waters at ~2 ka were a weak net sink for pCO_2 (ΔpCO_2 = -6 ppmv) and likely results from the interplay and change in the balance between a stronger 'biological pump' and a corresponding decrease in the contribution and/or intensity of upwelling and advection of CO_2-rich CDW. The increasing $\delta^{13}C_{adj}$ and $\Delta\delta^{13}C$ gradient (Fig. 5a, c) and the corresponding

increase in alkenone concentrations (Fig. 5d) from ~4.1 to 2 ka is indicative of increased primary productivity, and corresponds to a decrease in wind strength from ~4 to 1 ka[49,50].

Our findings demonstrate the interplay and changing balance between the removal of CO_2 by biological productivity in surface waters and CO_2 outgassing via circulation changes during the last G-IG rise in atmospheric CO_2. The modern Southern Ocean shows considerable zonal variability in annual and seasonal air-sea CO_2 flux[53], so such spatial heterogeneity in past ocean-atmosphere CO_2 exchange is not surprising. This study provides evidence that the CO_2 dynamics of Holocene surface waters in the Southern Ocean are dependent on competing factors such as the ocean's biological pump and changes in the location and intensity of SWW. The evolving relationship between atmospheric dynamics and carbon exchange is critically important for understanding the role of Southern Hemisphere winds in modulating the uptake of anthropogenic CO_2 (refs 54, 55).

References

1 Luthi, D. *et al.* High-resolution carbon dioxide concentration record 650,000-800,000 years before present. *Nature* **453**, 379-382 (2008).

2 Sigman, D. M., Hain, M. P. & Haug, G. H. The polar ocean and glacial cycles in atmospheric CO_2 concentration. *Nature* **466**, 47-55 (2010).

3 Ciais, P. *et al.* Large inert carbon pool in the terrestrial biosphere during the Last Glacial Maximum. *Nat Geosci* **5**, 74-79 (2011).

4 Ciais, P. *et al.* in *Climate Change 2013: The Physical Science Basis. Contribution of Working Group I to the Fifth Assessment Report of the Intergovernmental Panel on Climate Change* (ed T.F. Stocker, D. Qin, G.-K. Plattner, M. Tignor, S.K. Allen, J. Boschung, A. Nauels, Y. Xia, V. Bex and P.M. Midgley) (2013).

5 Winterfeld, M. *et al.* Deglacial mobilization of pre-aged terrestrial carbon from degrading permafrost. *Nat Commun* **9**, 3666 (2018).

6 Knox, F. & McElroy, M. B. Changes in atmospheric CO_2: Influence of the marine biota at high latitude. *J. Geophys. Res.* **89**, 4629-4637 (1984).

7 Sarmiento, J. L. & Toggweiler, J. R. A new model for the role of the oceans in determining atmospheric pCO_2. *Nature* **308**, 621-624 (1984).

8 Siegenthaler, U. & Wenk, T. Rapid atmospheric CO_2 variations and ocean circulation. *Nature* **308**, 624-627 (1984).

9 Sigman, D. M. & Boyle, E. A. Glacial/interglacial variations in the atmospheric carbon dioxide. *Nature* **407**, 859-869 (2000).

10 Toggweiler, J. R., Russell, J. L. & Carson, S. R. Midlatitude westerlies, atmospheric CO_2, and climate change during ice ages. *Paleoceanography* **21**, 10.1029/2005PA001154 (2006).

11 Anderson, R. F., Chase, Z., Fleisher, M. Q. & Sachs, J. The Southern Ocean's biological pump during the Last Glacial Maximum. *Deep Sea Res. Part II* **49**, 1909-1938 (2002).

12 Skinner, L. C. *et al.* Ventilation of the deep Southern Ocean and deglacial CO_2 rise. *Science* **328**, 1147-1151 (2010).

13 Burke, A. & Robinson, L. F. The Southern Ocean's role in carbon exchange during the last deglaciation. *Science* **335**, 557-561 (2012).

14 Martínez-García, A. *et al.* Iron fertilization of the subantarctic ocean during the last ice age. *Science* **343**, 1347-1350 (2014).

15 Martínez-Botí, M. A. *et al.* Boron isotope evidence for oceanic carbon dioxide leakage during the last deglaciation. *Nature* **518**, 219-222 (2015).

16 Jaccard, S. L., Galbraith, E. D., Martínez-García, A. & Anderson, R. F. Covariation of deep Southern Ocean oxygenation and atmospheric CO_2 through the last ice age. *Nature* **530**, 207-210 (2016).

17 Ronge, T. A. *et al.* Radiocarbon constraints on the extent and evolution of the South Pacific glacial carbon pool. *Nat Commun* **7**, 11487 (2016).

18 Kohfeld, K. E. & Chase, Z. Temporal evolution of mechanisms controlling ocean carbon uptake during the last glacial cycle. *Earth Planet. Sci. Lett.* **472**, 206-215 (2017).

19 Rae, J. W. B. *et al.* CO_2 storage and release in the deep Southern Ocean on millennial to centennial timescales. *Nature* **562**, 569-573 (2018).

20 Locarnini, R. A. *et al. World Ocean Atlas 2013, Volume 1: Temperature. S. Levitus, Ed.; A. Mishonov, Technical Ed.*, (2013).

21 Conkright, M., Levitus, S. & Boyer, T. *The World Ocean Atlas 1994 Volume 1: Nutrients*. (US Department of Commerce, 1994).

22 Sikes, E. L. *et al.* Southern Ocean seasonal temperature and Subtropical Front movement on the South Tasman Rise in the late Quaternary. *Paleoceanography* **24**, 10.1029/2008PA001659 (2009).

23 Schrag, D. P. *et al.* The oxygen isotopic composition of seawater during the Last Glacial Maximum. *Quat. Sci. Rev.* **21**, 331-342 (2002).

24 Spero, H. J., Bijma, J., Lea, D. W. & Bemis, B. E. Effect of seawater carbonate concentration on foraminiferal carbon and oxygen isotopes. *Nature* **390**, 497-500 (1997).

25 Bemis, B. E., Spero, H. J., Bijma, J. & Lea, D. W. Reevaluation of the oxygen isotopic composition of planktonic foraminifera: Experimental results and revised paleotemperature equations. *Paleoceanography* **13**, 150-160 (1998).

26 Bemis, B. E., Spero, H. J., Lea, D. W. & Bijma, J. Temperature influence on the carbon isotopic composition of *Globigerina bulloides* and *Orbulina universa* (planktonic foraminifera). *Mar. Micropaleontol.* **38**, 213-228 (2000).

27 Barker, S. & Elderfield, H. Foraminiferal calcification response to Glacial-Interglacial changes in atmospheric CO_2. *Science* **297**, 833-836 (2002).

28 Bijma, J., Honisch, B. & Zeebe, R. E. Impact of the ocean carbonate chemistry on living foraminiferal shell weight: Comment on "Carbonate ion concentration in glacial-age deep waters of the Caribbean Sea" by W.S. Broecker and E. Clark. *Geochem. Geophys, Geosyst.* **3**, 1064, 1010.1029/2002GC000388 (2002).

29 Foster, G. L. & Rae, J. W. B. Reconstructing Ocean pH with Boron Isotopes in Foraminifera. *Annu. Rev. Earth Planet. Sci.* **44**, 207-237 (2016).

30 Broecker, W. S. & Clark, E. Glacial to Holocene redistribution of carbonate ion in the deep sea. *Science* **294**, 2152-2155 (2001).

31 Moy, A. D., Howard, W. R., Bray, S. G. & Trull, T. W. Reduced calcification in modern Southern Ocean planktonic foraminifera. *Nat Geosci* **2**, 276-280 (2009).

32 Raitzsch, M. *et al.* Boron isotope-based seasonal paleo-pH reconstruction for the Southeast Atlantic – A multispecies approach using habitat preference of planktonic foraminifera. *Earth Planet. Sci. Lett.* **487**, 138-150 (2018).

33 Bereiter, B. *et al.* Revision of the EPICA Dome C CO_2 record from 800 to 600 kyr before present. *Geophys. Res. Lett.* **42**, 542-549 (2015).

34 Shoenfelt, E. M. *et al.* Highly bioavailable dust-borne iron delivered to the Southern Ocean during glacial periods. *Proc. Natl. Acad. Sci. U.S.A.*, 10.1073/pnas.1809755115 (2018).

35 Kumar, N. *et al.* Increased biological productivity and export production in the glacial Southern Ocean. *Nature* **378**, 675-680 (1995).

36 Elderfield, H. & Rickaby, R. E. M. Oceanic Cd/P ratio and nutrient utilization in the glacial Southern Ocean. *Nature* **405**, 305-310 (2000).

37 Chase, Z., Anderson, R. F., Fleisher, M. Q. & Kubik, P. W. Accumulation of biogenic and lithogenic material in the Pacific sector of the Southern Ocean during the past 40,000 years. *Deep Sea Res. Part II: Top. Stud. Oceanogr.* **50**, 799-832 (2003).

38 Francois, R. *et al.* Contribution of Southern Ocean surface-water stratification to low atmospheric CO_2 concentrations during the Last Glacial Period. *Nature* **389**, 929-935 (1997).

39 Abelmann, A. *et al.* The seasonal sea-ice zone in the glacial Southern Ocean as a carbon sink. *Nat Commun* **6**, 8136 (2015).

40 Basak, C. *et al.* Breakup of last glacial deep stratification in the South Pacific. *Science* **359**, 900-904 (2018).

41 Sikes, E. L., Cook, M. S. & Guilderson, T. P. Reduced deep ocean ventilation in the Southern Pacific Ocean during the last glaciation persisted into the deglaciation. *Earth Planet. Sci. Lett.* **438**, 130-138 (2016).

42 Kohfeld, K. E., Quéré, C. L., Harrison, S. P. & Anderson, R. F. Role of marine biology in glacial-interglacial CO_2 cycles. *Science* **308**, 74-78 (2005).

43 Broecker, W. S. & Peng, T.-H. *Tracers in the Sea.* (Eldigio Press, 1982).

44 Volk, T. & Hoffert, M. I. in *The Carbon Cycle and Atmospheric CO_2: Natural Variations Archean to Present Geophys. Monogr.* (eds E. Sundquist & W.S. Broecker) 99-110 (AGU, 1985).

45 Villanueva, J. *et al.* A latitudinal productivity band in the central North Atlantic over the last 270 kyr: An alkenone perspective. *Paleoceanography* **16**, 617-626 (2001).

46 Pailler, D. *et al.* Burial of redox-sensitive metals and organic matter in the equatorial Indian Ocean linked to precession. *Geochim. Cosmochim. Acta* **66**, 849-865 (2002).

47 Ziegler, M., Diz, P., Hall, I. R. & Zahn, R. Millennial-scale changes in atmospheric CO_2 levels linked to the Southern Ocean carbon isotope gradient and dust flux. *Nat Geosci* **6**, 457-461 (2013).

48 Hasenfratz, A. P. *et al.* The residence time of Southern Ocean surface waters and the 100,000-year ice age cycle. *Science* **363**, 1080-1084 (2019).

49 Moreno, P. I., Francois, J. P., Moy, C. M. & Villa-Martínez, R. Covariability of the Southern Westerlies and atmospheric CO_2 during the Holocene. *Geology* **38**, 727-730 (2010).

50 Saunders, K. M. *et al.* Holocene dynamics of the Southern Hemisphere westerly winds and possible links to CO_2 outgassing. *Nature Geosci* **11**, 650-655 (2018).

51 Anderson, R. F. *et al.* Wind-driven upwelling in the Southern Ocean and the deglacial rise in atmospheric CO_2. *Science* **323**, 1443-1448 (2009).

52 Spero, H. J. & Lea, D. W. The cause of carbon isotope minimum events on glacial terminations. *Science* **296**, 522-525 (2002).

53 Takahashi, T. *et al.* The changing carbon cycle in the Southern Ocean. *Oceanography* **25**, 26-37 (2012).

54 Le Quéré, C. *et al.* Saturation of the Southern Ocean CO_2 sink due to recent climate Change. *Science* **316**, 1735-1738 (2007).

55 Landschützer, P. *et al.* The reinvigoration of the Southern Ocean carbon sink. *Science* **349**, 1221-1224 (2015).

Correspondence and request for materials should be addressed to A.D.M (email: Andrew.Moy@aad.gov.au).

Acknowledgements

This work was supported by the Australian Antarctic Division (AAS 4061) and the Australian Government's Cooperative Research Centres Programme through the Antarctic Climate and Ecosystems Cooperative Research Centre (ACE CRC). The boron isotope analyses were supported by the European Union 5th Framework Programme project 6C (Project ID: EVK2-CT-2002-00135 6C). E.C. and C.P. acknowledge Graham Logan and Geoscience Australia for providing analytical facilities for alkenone analyses. We thank the French Polar Institute and the crew of the RV Marion Dufresne for their efforts in recovering sediment core MD972106.

Author contributions

A.D.M. and W.R.H. designed the study with input from M.R.P. and J.B. The manuscript was written by A.D.M., W.R.H., M.R.P. and J.B. with contributions from M.J.C., E.C., C.P., M.K.G., and T.B.C. Analysis and interpretation of the measurements was completed by

A.D.M., W.R.H., M.R.P., J.B., M.J.C., E.C., C.P., M.K.G., and T.B.C. All authors contributed towards improving the final manuscript.

Competing Interest

The authors declare no competing interests.

Supplementary Information is available in the online version of the paper.

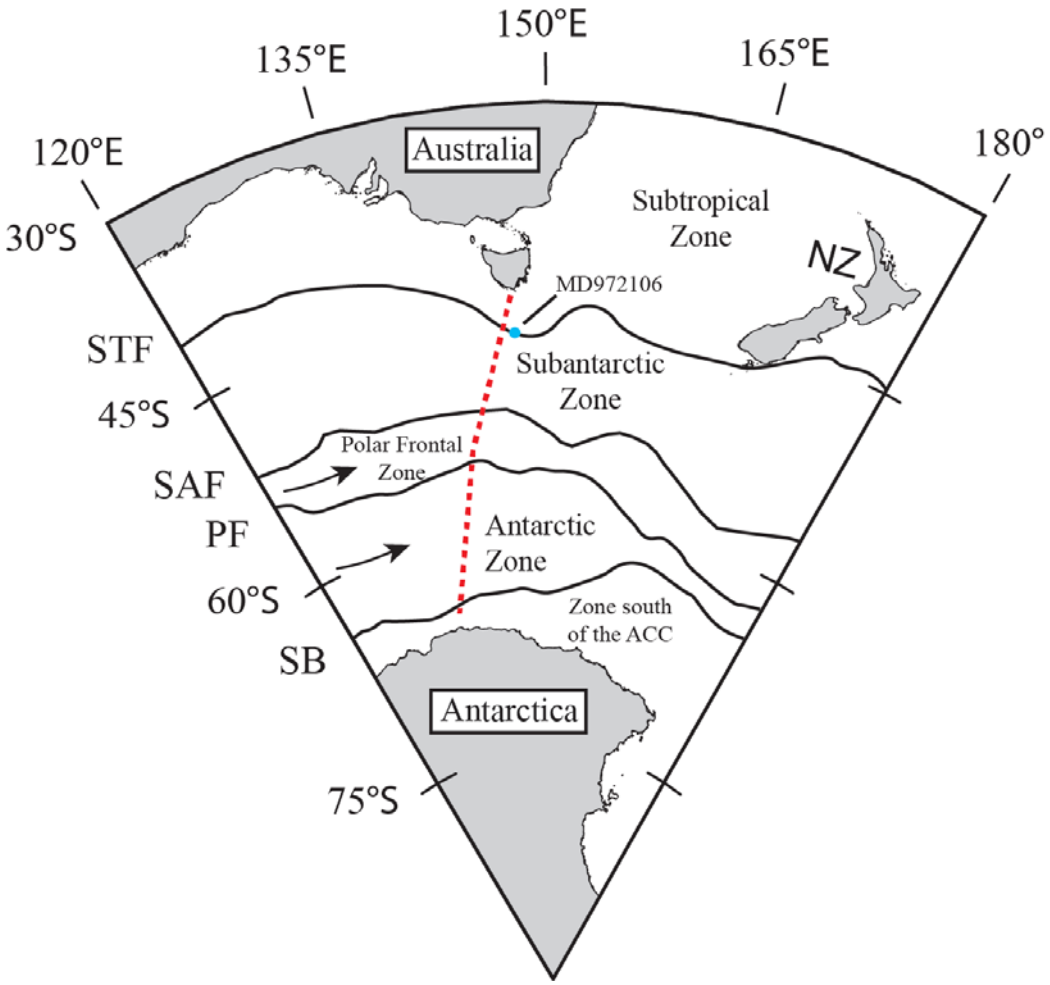

Figure 1. Location of the MD972106 sediment core and modern position of Southern Ocean water masses and fronts. MD972106 is located at 45°09'S, 146°17'E (water depth 3310 m). STF, Sub-Tropical Front; SAF, Sub-Antarctic Front; PF, Polar Front; SB, southern boundary of the Antarctic Circumpolar Current (ACC). Arrows are used to indicate the ACC direction. Dashed red line shows the repeat hydrographic transect between Tasmania and Antarctic along ~140° E (WOCE SR3 section line).

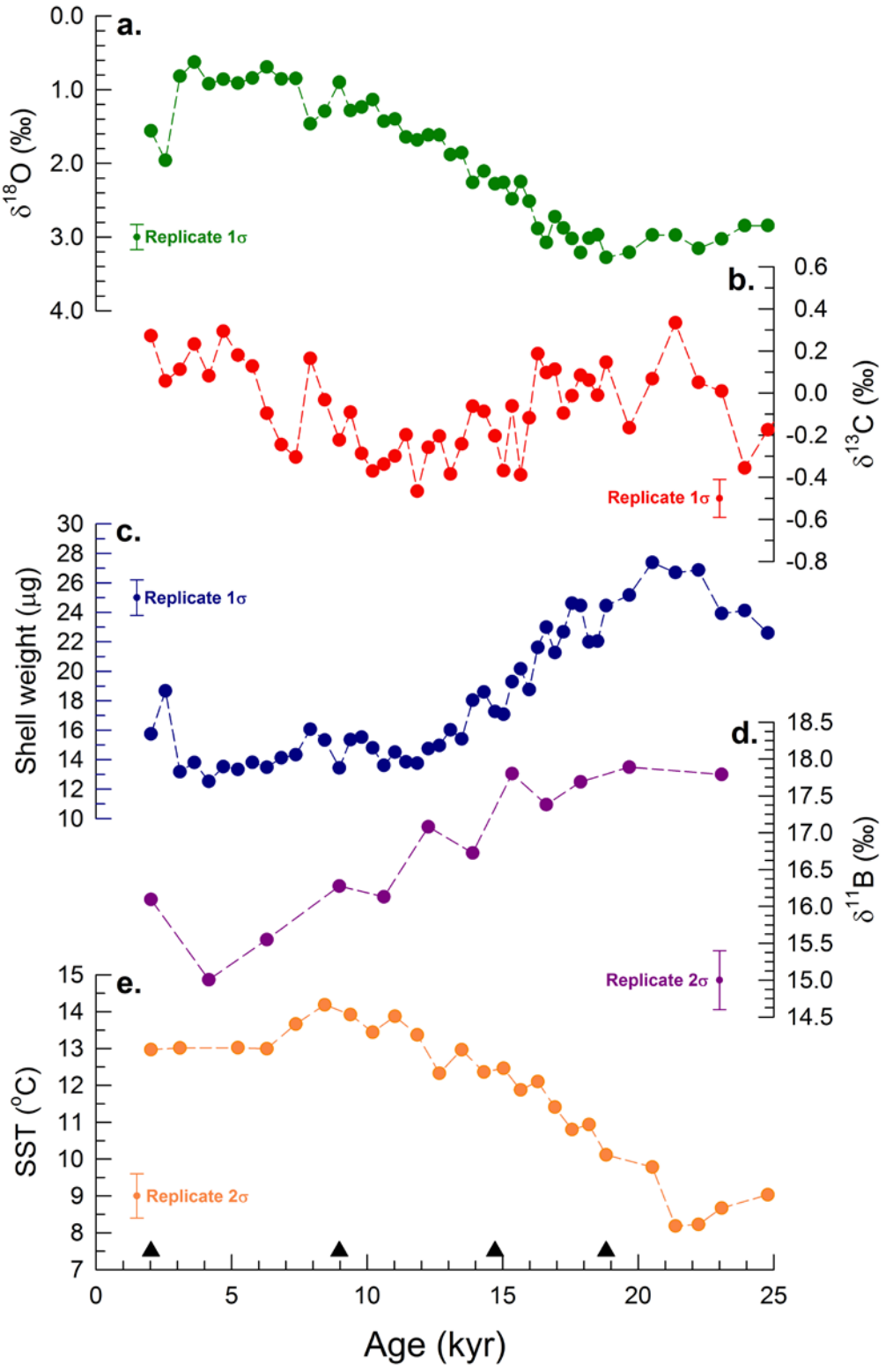

Figure 2. $\delta^{18}O$, $\delta^{13}C$, shell weight and $\delta^{11}B$ for the planktonic foraminifer, *Globigerina bulloides*, and palaeo SST estimates from alkenones in sediment core MD972106. Measured *G. bulloides* **a**, $\delta^{18}O$ (green circles), **b**, $\delta^{13}C$ (red circles), **c**, shell weight (blue circles) and **d**, $\delta^{11}B$ (purple circles). **e**, Palaeo SST estimates from MD972106 obtained from alkenones

unsaturation ratio ($U_{37}^{K\prime}$) (orange circles). Age model was constructed using calibrated ^{14}C ages (black triangles; Methods). Error bars represent 1σ uncertainties for $\delta^{18}O$, $\delta^{13}C$, and shell weight, and 2σ uncertainties for $\delta^{11}B$ based on replicate measurements (Methods). Error bars on palaeo SSTs represent the 2σ analytical uncertainty for replicate measurements on a homogenous laboratory (sediment) standard (Methods).

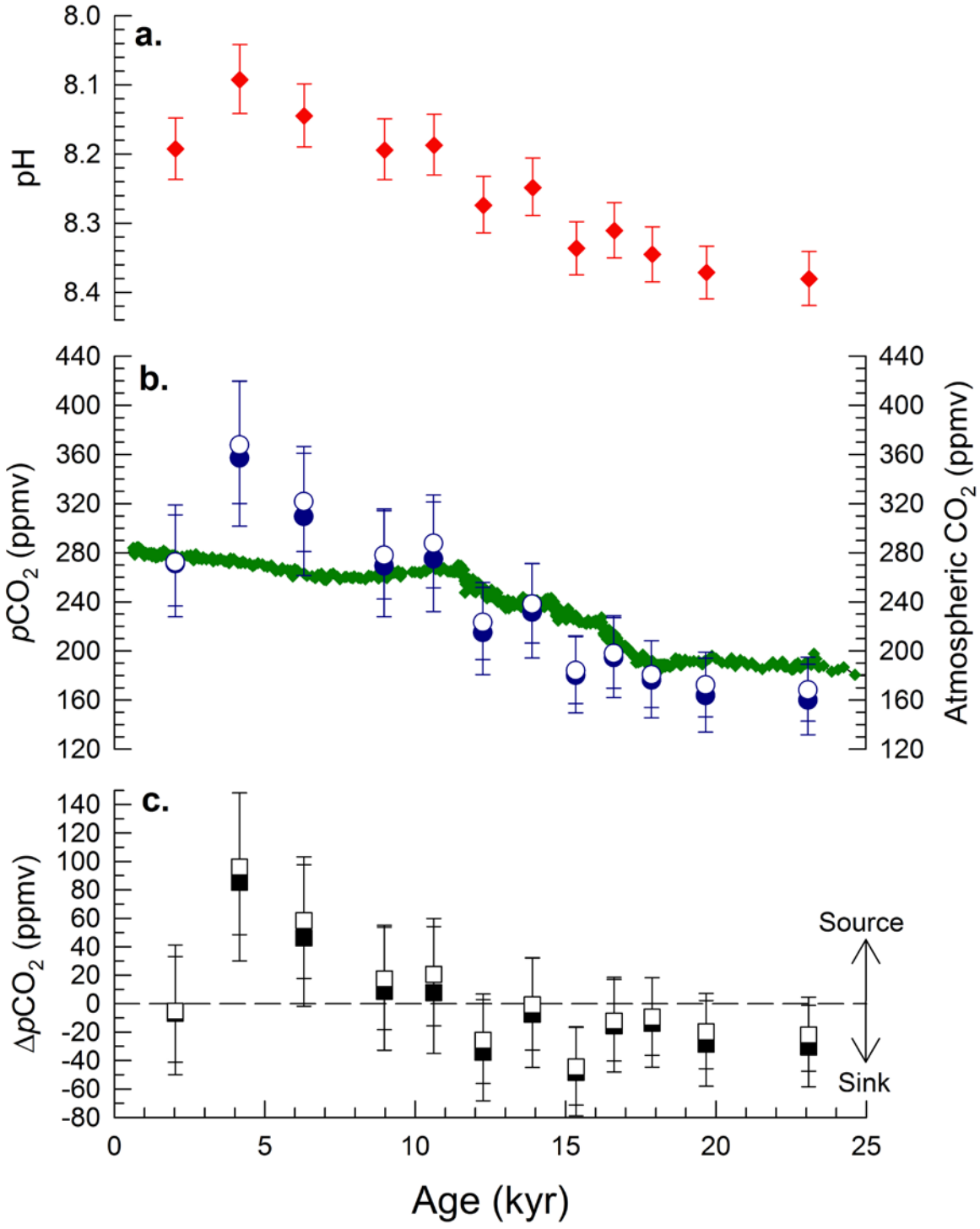

Figure 3. Reconstructed surface water pH and pCO_2 at the MD972106 site and atmospheric CO_2 over the past 25,000 years. **a,** Reconstructed surface water pH (red diamonds). **b,** Reconstructed pCO_2 calculated from pH, alkenone SST and alkalinity (Method 1; blue circles) and pCO_2 calculated from pH, alkenone SST and DIC (Method 2; blue open circles). Also shown is the atmospheric CO_2 record (Antarctic ice core CO_2 composite[33]; green

diamonds). **c,** ΔpCO_2 is the difference between reconstructed surface water pCO_2 (Method 1 (black squares); and Method 2 (black open squares)) and atmospheric CO_2 (Antarctic ice core CO2 composite[33]). Error bars in **a, b** and **c** represent 95% confidence intervals around the Monte Carlo mean, where 2σ uncertainties on the individual input variables and other carbonate system parameters are propagated via the Monte Carlo simulation (n = 10,000) in the statistical analysis program R (Methods).

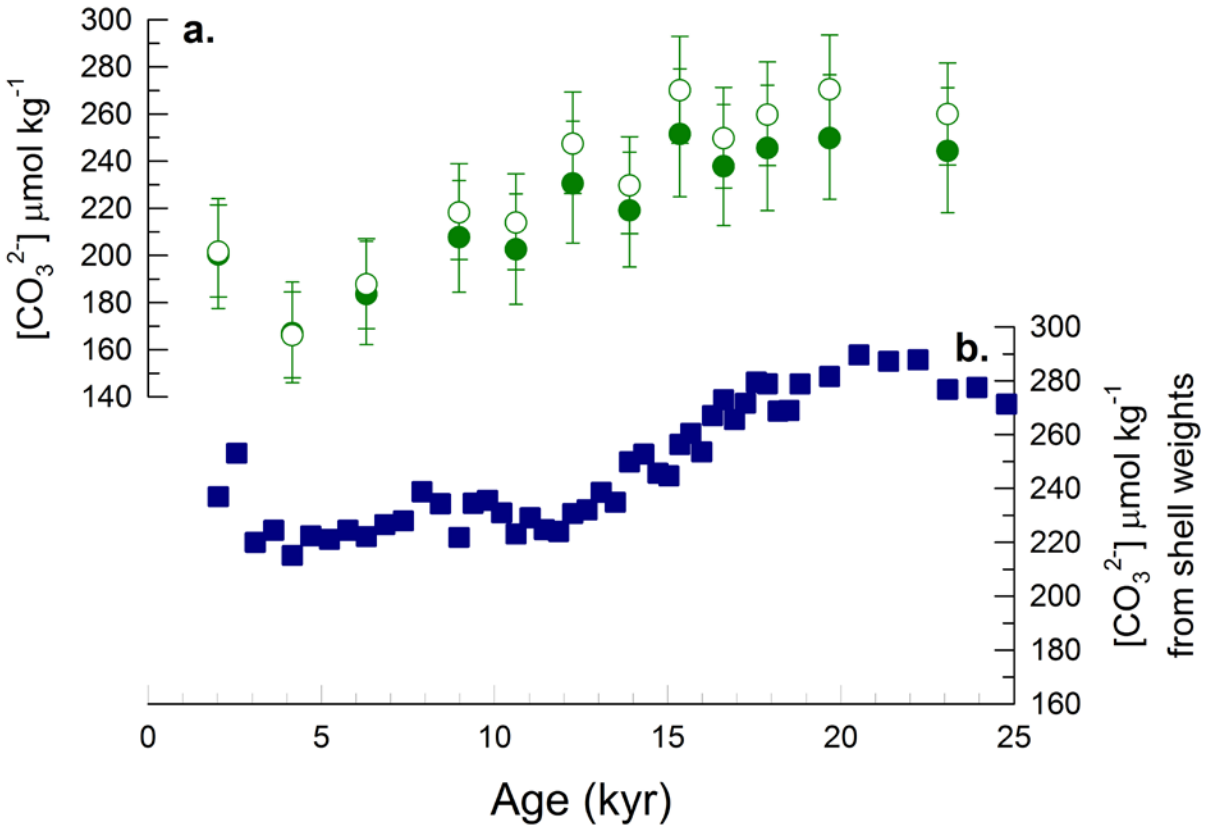

Figure 4. Reconstructed surface water carbonate ion concentration. **a**, $[CO_3^{2-}]$ from δ^{11}B-pH estimates, alkenone SST and alkalinity (Method 1; green circles), and from δ^{11}B-pH estimates, alkenone SST and DIC (Method 2; green open circles). **b**, $[CO_3^{2-}]$ from shell weight data (blue squares) using the shell weight-$[CO_3^{2-}]$ relationship[27]. Error bars in **a** represent 95% confidence intervals around the Monte Carlo mean, where 2σ uncertainties on the individual input variables and other carbonate system parameters are propagated via the Monte Carlo simulation (n = 10,000) in the statistical analysis program R (Methods).

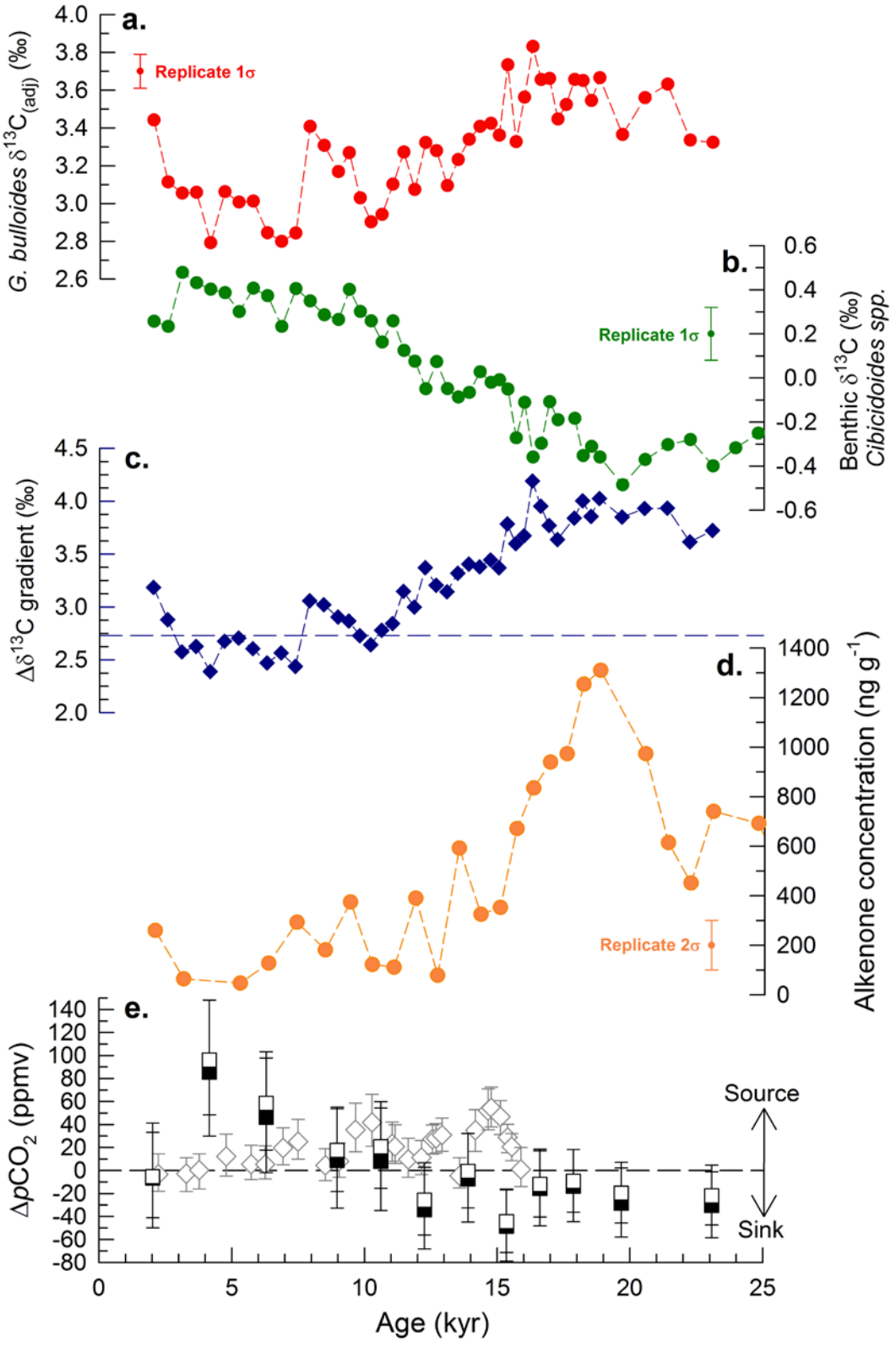

Figure 5. Planktonic and benthic foraminiferal $\delta^{13}C$, $\Delta\delta^{13}C$ gradient, alkenone concentrations and ΔpCO_2 over the past 25,000 years. **a**, *G. bulloides* $\delta^{13}C_{(adj)}$ (red circles), **b**, benthic $\delta^{13}C$ for *Cibicidoides spp.* (green circles), **c**, $\Delta\delta^{13}C$ gradient ($\Delta\delta^{13}C$

planktonic$_{(adj)}$ – benthic foraminifera); blue diamonds and blue dashed line shows the Holocene $\Delta\delta^{13}C$ gradient average, **d**, alkenone concentrations (orange circles), **e,** ΔpCO_2 differences between surface water pCO_2 and atmospheric CO_2 (from Antarctic ice core CO_2 composite[33]) as in Figure **3c**. Also shown in **e** is the calculated ΔpCO_2 for the Atlantic sector of SAZ[15] (sediment core PS2498-1 at 44.15°, 14.23°, 3,783m water depth; grey open diamonds and error bars are the 95% uncertainty bounds). In **a,** *G. bulloides* $\delta^{13}C$ are temperature and $[CO_3^{2-}]$ adjusted (Methods). Error bars in **a** and **b** represent 1σ uncertainties based on replicate measurements; error bars in **d** represent 2σ for replicate extractions and measurements on a homogenous laboratory (sediment) standard, and error bars in **e** represent 95% confidence intervals around the Monte Carlo mean, based on 2σ uncertainties on the individual input variables and other carbonate system parameters are propagated via the Monte Carlo simulation (n = 10,000) in the statistical analysis program R (Methods).

Methods

Materials and methods. Sediment core MD972106 (45°09'S, 146°17'E, water depth 3310 m) is a 32 m long piston core collected using the CALYPSO Kullenberg corer on board the RV *Marion Dufresne* in 1997 (in this paper, we present data from the top 2.5m of the core) and was recovered from the northern flank of the South Tasman Rise. The MD972106 site is located at the southern edge of the Subtropical front (STF) (Fig. 1) and modern bottom water covering the South Tasman Rise is Circumpolar Deep Water (CDW), a mixture of high $\delta^{13}C$ (low nutrient) NADW (or northern source deep-water) and re-circulated low $\delta^{13}C$ (high nutrient) deep-water from the Indian and Pacific Oceans (Supplementary Fig. 1).

MD972106 was sampled every 5 cm on board RV *Marion Dufresne*. Raw sediment samples were oven dried at 60°C, and then disaggregated in distilled water at the ACE CRC, University of Tasmania. Water saturated sediment samples were wet sieved through a >150 μm mesh. The dried >150 μm fraction was sieved to isolate the 300-355 μm fraction from which ≥50 planktonic foraminifera *Globigerina bulloides* were picked. We selected *G. bulloides* as this species shows a seasonal range in $\delta^{18}O$ values in this region of the Southern Ocean that is consistent with calcification in near-surface waters[56], and comparisons between flux-weighted sediment trap and surface sediment $\delta^{18}O$ values indicate the sedimentary record retains the seasonal isotopic imprint for *G. bulloides*[56].

Each batch of foraminifera was ultrasonically cleaned in methanol and oven dried at 60°C. Any broken tests were discarded. The cleaned samples were used to determine the average shell weights and isotopic compositions ($\delta^{18}O$, $\delta^{13}C$ and $\delta^{11}B$), with the shells undergoing further cleaning prior to determination of their $\delta^{11}B$ values. Average shell weight, $\delta^{18}O$ and $\delta^{13}C$ measurements were conducted at 5 cm intervals. Determination of $\delta^{11}B$ were made at 20 cm resolution.

Age model. Age control for MD972106 is based on accelerator mass spectrometry (AMS) radiocarbon (^{14}C) dating of the planktonic foraminifer, *Globorotalia inflata*. Five published AMS ^{14}C dates for MD972106 (ref. 57) were recalibrated to calendar ages using the Calib 7.1 program[58] with the Marine13 data set[59]. Ages were corrected for the local ^{14}C reservoir correction (ΔR) for surface waters in this region of the Southern Ocean using a constant ΔR regional mean value (ΔR = 107±13 yr) calculated for the Chatham Islands from the marine reservoir correction database[60]. The ΔR (107±13 yr) incorporates the measured ^{14}C age of 560±40 yrBP obtained from gastropods[61]. Using a different and older ΔR for the ^{14}C dates at 16.1 ka and 23.5 ka would slightly change the chronology, but this would not affect the conclusions of our study for the LGM and early deglacial periods. For example, using a ΔR = 900 yr for the ^{14}C dates at 16.1 ka and 23.5 ka would change the chronology by ~0.8 - 0.9 kyr, and using a ΔR = 900 yr for the ^{14}C date at 16.1 ka and a ΔR = 1500 yr for ^{14}C date at 23.5 ka, would change the chronology by ~0.8 to 1.4 ka. The average sedimentation rate at MD972106 was ~9.3 cm kyr^{-1} over the past 25 kyr.

Stable isotope analyses. Oxygen ($\delta^{18}O$) and carbon ($\delta^{13}C$) isotope ratios were determined for the planktonic foraminifera, *G. bulloides* (300–355 μm), and the benthic foraminiferal taxa *Cibicidoides spp.* (from the >150 μm size fraction). Measurements of $\delta^{18}O$ and $\delta^{13}C$ were conducted on an automated individual–carbonate reaction Kiel Device coupled to a Finnigan MAT-251 isotope ratio mass spectrometer at the Research School of Earth Sciences, ANU. Calcite samples weighing ~200 μg were reacted with 103% phosphoric acid at 90°C to liberate sufficient CO_2 for isotopic analysis. The $\delta^{18}O$ and $\delta^{13}C$ values are reported as per mil (‰) deviations relative to the Vienna Peedee Belemnite (VPDB) standard. The results have been normalised on the VPDB scale such that the NBS-19 calcite standard yields $\delta^{18}O$ VPDB (−2.20 ‰) and $\delta^{13}C$ VPDB (+1.95 ‰) and NBS-18 yields $\delta^{18}O$ VPDB (−23.0 ‰) and $\delta^{13}C$ VPDB

(−5.0 ‰). The 2σ uncertainties for replicate in-run measurements of NBS-19 (n=197) were ±0.05 ‰ and ±0.02 ‰ for $\delta^{18}O$ and $\delta^{13}C$, respectively. The average standard deviation for repeat measurement of two planktonic samples was ±0.17 ‰ for $\delta^{18}O$ and ±0.09 ‰ for $\delta^{13}C$, and for benthic samples was ±0.05 ‰ for $\delta^{18}O$ and ±0.12 ‰ for $\delta^{13}C$.

Boron isotope ($\delta^{11}B$) values were determined for the planktonic foraminifera, *G. bulloides* (300-355 μm) at Southampton University using previously described methods[62-64]. Oxidative cleaning procedures followed those in Barker *et al.*, (ref. 65). We analysed ten *G. bulloides* (150–250 μg of calcite) for each in-run measurement and this provided ~2–3 ng of boron. The average 2σ in-run measurement precision was <0.2 ‰. The average agreement of repeat measurements on separate sample aliquots was ±0.4 ‰ (n = 7) and the average external 2σ precision is, at most, ±0.4 ‰. Foraminiferal cleaning procedures[65] were verified for all samples by Al/Ca ratios <100 μmol mol^{-1} and this provides a sufficient screen against clay contamination[66].

Planktonic foraminifera shell weights. *G. bulloides* shell weights were determined by picking 50 or more whole individual shells from the 300-355μm size fraction. Each batch of whole foraminiferal shells were ultrasonically cleaned in methanol and oven dried at 60°C. Any shells broken during the cleaning process were discarded and the remaining shells were counted. The shells were weighed on a microbalance (precision = 0.1 μg) and average shell weights were calculated by dividing the measured weight by the total number of whole foraminifera. Replicate shell-weight measurements were determined by selecting a separate aliquot of 50 or more shells from the same sample. The mean difference of replicate shell weights is ±1.2 μg (1σ; n = 55).

Palaeo sea surface temperature (SST) and alkenone concentrations. Alkenones were analyzed at Geoscience Australia following the methods of Calvo *et al.*, (ref. 67) and, with

them, SST estimates were obtained from the alkenone unsaturation ratio ($U_{37}^{K'}$ index). Alkenone concentrations were quantified by using *n*-hexatriacontane as an internal standard. The standard deviation for alkenone concentrations is 50 ng g^{-1} (2σ; replicate extractions and measurements of a homogenous laboratory sediment standard). Alkenone-derived SSTs were reconstructed using the $U_{37}^{K'}$-SST relationship of Müller *et al.*, (ref. 68) where $U_{37}^{K'}$ = 0.033 x SST + 0.044 for annually averaged SSTs. $U_{37}^{K'}$ measurements were completed at 10 cm sample resolution. The standard deviation for replicate measurements of a homogenous laboratory (sediment) standard is, at the most ±0.6 °C (2σ). The standard error of SST estimates from the $U_{37}^{K'}$-SST calibration[68] is ±1.5 °C. Long-term climate data from the World Ocean Atlas 2013 (WOA13; 0.25°)[69] gives a modern annual SST of 12.3 ºC at the MD972106 locality, which is close to the most recent core-top sediment $U_{37}^{K'}$ derived SST of 13.0 °C.

Reconstruction of surface water *p*CO_2. Seawater *p*CO_2 can be calculated from temperature, salinity and pressure, and knowledge of two out of the six main carbonate system parameters (free aqueous carbon dioxide ($CO_{2(aq)}$), bicarbonate ion (HCO_3^-), carbonate ion (CO_3^{2-}), hydrogen ion (H^+), dissolved inorganic carbon (DIC), and total alkalinity (TA)). Accordingly, past changes in seawater *p*CO_2 can be calculated using estimates of seawater pH and either DIC or TA. Here, we use an alkenone-based proxy for seawater temperature, planktonic foraminiferal $\delta^{11}B$ to estimate pH, planktonic foraminiferal $\delta^{13}C$ to estimate DIC, and salinity derived seawater alkalinity to constrain major parameters of the seawater carbonate system. Past variations in sea surface water pH at the site of MD972106 are calculated from a recently published $\delta^{11}B$-pH relationship for *G. bulloides*[70] and the alkenone SST record. The $\delta^{11}B$-pH relationship for *G. bulloides*[70] expands on the previously published $\delta^{11}B$-pH relationship for the same species[71]. The $\delta^{11}B$-pH relationship[70] is similar to and within error of a previously published $\delta^{11}B$-pH relationship[71]. Even though the calibration uncertainty for Martínez-Botí

et al., (ref. 71) is considerably lower than Raitzsch *et al*., (ref. 70), we used the extended δ^{11}B-pH relationship data set for *G. bulloides*[70].

Variations in surface water pCO_2 (Fig. 3b) over the past 25 kyr are estimated using the SST alkenone record, the δ^{11}B surface water pH record and estimates of either alkalinity or DIC. One set of estimates is derived from δ^{11}B-based pH and seawater alkalinity, assuming that past variations in alkalinity were proportional to salinity, which can be estimated from past sea level [62,72] (Method 1) (Fig. 3a). An alternative set of estimates is derived from δ^{11}B-based pH, and foraminiferal δ^{13}C-based DIC (Method 2) (Fig. 3a). Both approaches use a Monte Carlo method to calculate pCO_2 from pH, DIC, salinity and temperature. This method generates quasi-normally distributed errors around central values with 10,000 repetitions, and sea water carbonate system calculations using the R-based[73] seacarb package[74]. 2σ uncertainties on the individual input variables and other carbonate system parameters are included to the end; δ^{11}B (±0.4 ‰), $U_{37}^{K\prime}$-derived SST (±1.0 °C), salinity (± 3psu), ALK (±200 μmol kg^{-1}), and DIC (±76 μmol kg^{-1}). A disequilibrium uncertainty ±20 ppm (2σ) is also included. Although we note the importance of propagating all the uncertainties, we also note that pH is by far the dominant variable on pCO_2, and that pH is well constrained by δ^{11}B alone[75]. Thus we are very confident that the change in pCO_2 forcing over this time is much more robust than the pCO_2 change in terms of absolute uncertainty[75]. The average pCO_2 difference between calculations using Method (1) and (2) is ~7 ppm.

Surface water pCO_2 and hence ocean circulation and productivity exerts an important control on atmospheric CO_2 levels. However, the difference between the two (ΔpCO_2) is also affected by terrestrial components of the carbon cycle such as (re-) growth of biomass or the dynamics of (coastal) permafrost. Hence, more important than the absolute magnitude of ΔpCO_2 is the change in this value, because this provides direct information as to whether a

particular area of the ocean was more or less important in driving the direction of atmospheric change. Thus, while there are intervals in our record where the analytical and/or age uncertainties preclude us from being certain whether our study area was acting as source or sink of CO_2 to the atmosphere, we can be confident that the change in surface water ΔpCO_2 levels in this area of the Southern Ocean made an important contribution to the last deglacial atmospheric CO_2 rise.

We used the total pH scale, equilibrium constants for the dissociation of carbonic acid from Dickson (ref. 76) and the boron isotope equilibrium constant from Klochko (ref. 77). Modern silicate and phosphate values were applied to the calculations but they had very little effect on the final results[78]. The proxies recorded in *G. bulloides* and in coccolithophorid alkenones predominantly reflect austral spring conditions in the region, because this is the seasonal maximum of production for both taxa[56,79]. Thus, the estimates of pCO_2 likely reflect austral spring conditions.

The calculated pCO_2 from boron isotope-based pH estimates and DIC (Method 2) utilizes an estimate of surface water DIC over time and requires a DIC estimate for the most recent sediment sample. The WOCE SR3 section line between 44° S and 46° S (ref. 80-82) indicates a modern surface water DIC of ~2061 µeq kg^{-1} at this site, where *G. bulloides* are known to calcify[56]. Estimates of DIC are then varied over time as a function of *G. bulloides* $\delta^{13}C$, with the difference between modern surface- and deep-water DIC derived via the difference between planktonic and benthic foraminiferal $\delta^{13}C$ (i.e. $\Delta DIC_{SW\text{-}DW}$ is proportional to $\Delta\delta^{13}C_{\text{ planktonic-benthic}}$). The biological drivers of surface-water $\delta^{13}C$ are mainly modulated by organic carbon production; carbonate precipitation does not significantly fractionate surface-water DIC. Therefore, any changes in the $CaCO_3$:C_{org} rain ratio would have a minor effect on DIC. Studies of the mechanisms of modulation of DIC in surface waters in this region (e.g.

ref. 83) and of the Southern Ocean more broadly (e.g. ref. 84), suggest the $CaCO_3$:C_{org} rain ratio is very low, with only a minor effect on surface DIC and surface $\delta^{13}C_{DIC}$. Any changes to the rain ratio would also affect surface-water pH, which we estimate through boron isotopes. Modern surface and deep water DIC are from WOCE line SR3 section between 44° S and 46° S (ref. 80-82), $\delta^{13}C_{SW}$ from King and Howard (ref. 85) and $\delta^{13}C_{DW}$ are from Moy *et al*., (ref. 57).

***G. bulloides* temperature- and $[CO_3^{2-}]$-adjusted $\delta^{13}C$ ($\delta^{13}C_{adj}$)**. Temperature and carbonate ion concentration ($[CO_3^{2-}]$) have an additional, often neglected, effect on planktonic foraminiferal $\delta^{13}C$ (refs 85,86, 87). For Method 2, temperature and $[CO_3^{2-}]$ adjustments on *G. bulloides* $\delta^{13}C$ used to estimate DIC do not significantly change the pCO_2 estimates. The average difference in pCO_2 estimates calculated from (a) boron isotope-based pH estimates and DIC (where *G. bulloides* $\delta^{13}C$ is not temperature and $[CO_3^{2-}]$-adjusted) and (b) boron isotope-based pH estimates and DIC (where *G. bulloides* $\delta^{13}C$ is temperature- and $[CO_3^{2-}]$-adjusted) is ~2 ppm (Supplementary Fig. 4). *G. bulloides* $\delta^{13}C$ values are adjusted for temperature using the $\delta^{13}C$ disequilibrium- temperature relation 0.11‰ $°C^{-1}$ (ref. 87). The $\delta^{13}C$ disequilibrium-temperature[87] relation we apply here is similar to the relationship estimated from a Southern Ocean sediment trap field study[85]. Temperature adjustments are made using the alkenone-based SST estimates in MD972106. *G. bulloides* $\delta^{13}C$ values are also adjusted for the so called carbonate ion ($[CO_3^{2-}]$) effect using the relationship between $\delta^{13}C$ disequilibrium and $[CO_3^{2-}]$ (-0.014‰ $[CO_3^{2-}]^{-1}$) (ref. 86). Estimates of $[CO_3^{2-}]$ are from surface water pCO_2 calculations that use boron isotope-based pH estimates and estimates of seawater alkalinity (Method 1). The 'close agreement' between the $[CO_3^{2-}]$ outputs from Method 1 and 2 (Fig. 4a) would yield a similar adjustment to *G. bulloides* $\delta^{13}C$ in terms of $[CO_3^{2-}]$ adjustments.

Data availability

All data are archived at the Australian Antarctic Data Centre (AADC) and are publicly accessible at AADC reference link.

References

56 King, A. L. & Howard, W. R. $\delta^{18}O$ seasonality of planktonic foraminifera from the Southern Ocean sediment traps: Latitudinal gradients and implications for paleoclimate reconstructions. *Mar. Micropal.* **56**, 1-24 (2005).

57 Moy, A. D., Howard, W. R. & Gagan, M. K. Late Quaternary palaeoceanography of the Circumpolar Deep Water from the South Tasman Rise. *J. Quat. Sci.* **21**, 763-777 (2006).

58 Stuiver, M., Reimer, P. J. & Reimer, R. W. CALIB 7.1 [WWW program] at http://calib.org. (2018).

59 Reimer, P. J. *et al.* IntCal13 and marine13 radiocarbon age calibration curves 0–50,000 years cal BP. *Radiocarbon* **55**, 1869-1887 (2013).

60 Reimer, P. J. & Reimer, R. W. A marine reservoir correction database and on-line interface. *Radiocarbon* **43**, 461-463 (2001).

61 Sikes, E. L., Samson, C. R., Guilderson, T. P. & Howard, W. R. Old radiocarbon ages in the southwest Pacific Ocean during the last glacial period and deglaciation. *Nature* **405**, 555-559 (2000).

62 Palmer, M. R. *et al.* Multi-proxy reconstruction of surface water pCO_2 in the northern Arabian Sea since 29 ka. *Earth Planet. Sci. Lett.* **295**, 49-57 (2010).

63 Palmer, M. R. & Pearson, P. N. A 23,000-year record of surface pH and pCO_2 in the Western Equatorial Pacific Ocean. *Science* **300**, 480-482 (2003).

64 Palmer, M. R., Pearson, P. N. & Cobb, S. J. Reconstructing past ocean pH-depth profiles. *Science* **282**, 1468-1471 (1998).

65 Barker, S., Greaves, M. & Elderfield, H. A study of cleaning procedures used for foraminiferal Mg/Ca paleothermometry. *Geochem. Geophys, Geosyst.* **4**, 10.1029/2003GC000559 (2003).

66 Rae, J. W. B., Foster, G. L., Schmidt, D. N. & Elliott, T. Boron isotopes and B/Ca in benthic foraminifera: Proxies for the deep ocean carbonate system. *Earth Planet. Sci. Lett.* **302**, 403-413 (2011).

67 Calvo, E., Pelejero, C. & Logan, G. A. Pressurized liquid extraction of selected molecular biomarkers in deep sea sediments used as proxies in paleoceanography. *J. Chromatogr. A* **989**, 197-205 (2003).

68 Müller, P. J. *et al.* Calibration of the alkenone paleotemperature index $U^{K'}_{37}$ based on core-tops from the eastern South Atlantic and the global ocean (60°N-60°S). *Geochim. Cosmochim. Acta* **62**, 1757-1772 (1998).

69 Locarnini, R. A. *et al. World Ocean Atlas 2013, Volume 1: Temperature. S. Levitus, Ed.; A. Mishonov, Technical Ed.*, (2013).

70 Raitzsch, M. *et al.* Boron isotope-based seasonal paleo-pH reconstruction for the Southeast Atlantic – A multispecies approach using habitat preference of planktonic foraminifera. *Earth Planet. Sci. Lett.* **487**, 138-150 (2018).

71 Martínez-Botí, M. A. *et al.* Boron isotope evidence for oceanic carbon dioxide leakage during the last deglaciation. *Nature* **518**, 219-222 (2015).

72 Waelbroeck, C. *et al.* Sea-level and deep water temperature changes derived from benthic foraminifera isotopic records. *Quat. Sci. Rev.* **21**, 295-305 (2002).

73 R Development Core Team. A language and environment for statistical computing (R Foundation for Statistical Computing, Vienna, Austria). URL http://www.R-project.org/. (2013).

74 Gattuso, J.-P. Seacarb: Seawater carbonate chemistry with R. R package version 3.1.1. Available at https://cran.r-project.org/package=seacarb. (2011).

75 Hain, M. P., Foster, G. L. & Chalk, T. Robust Constraints on Past CO_2 Climate Forcing From the Boron Isotope Proxy. *Paleoceanogr Paleoclimatol* **33**, 1099-1115 (2018).

76 Dickson, A. G. Thermodynamics of the dissociation of boric acid in synthetic seawater from 273.15 to 318.15 K. *Deep Sea Research Part A. Oceanographic Research Papers* **37**, 755-766 (1990).

77 Klochko, K. *et al.* Experimental measurement of boron isotope fractionation in seawater. *Earth Planet. Sci. Lett.* **248**, 276-285 (2006).

78 Lauvset, S. K. *et al.* A new global interior ocean mapped climatology: the $1° \times 1°$ GLODAP version 2. *Earth Syst. Sci. Data* **8**, 325-340 (2016).

79 Sikes, E. L., O'Leary, T., Nodder, S. D. & Volkman, J. K. Alkenone temperature records and biomarker flux at the subtropical front on the chatham rise, SW Pacific Ocean. *Deep Sea Res. Part I Oceanogr. Res. Pap.* **52**, 721-748 (2005).

80 Tilbrook, B. & Rintoul, S. Hydrographic, chemical and total CO_2 data obtained during RSV *Aurora Australis* in the Southern Pacific Ocean during WOCE section P12 (SR3/S04, EXPOCODE 09AR9404_1), (13 December, 1994 - 02 February, 1995). http://cdiac.ornl.gov/ftp/oceans/p12woce/. Carbon Dioxide Information Analysis Center, Oak Ridge National Laboratory, US Department of Energy, Oak Ridge, Tennessee. (1995).

81 Tilbrook, B., Rintoul, S. & Sabine, C. L. Carbon dioxide, hydrographic and chemical data obtained during R/V *Aurora Australis* repeat hydrography cruise in the Southern

Ocean: CLIVAR CO_2 repeat section SR03_2001 (EXPOCODE AA0301), (29 October - 22 November, 2001). http://cdiac.ornl.gov/ftp/oceans/CLIVAR/SR03_AA0301_2001.data/. Carbon Dioxide Information Analysis Center, Oak Ridge National Laboratory, US Department of Energy, Oak Ridge, Tennessee. (2001).

82 Tilbrook, B., McNeil, B. & Rosenberg, M. Hydrographic, chemical and carbon data obtained during RSV *Aurora Australis* in the Southern Pacific Ocean during WOCE section SR03, (EXPOCODE 09AR19980228), (28 February - 01 April, 1988). http://cdiac.ornl.gov/ftp/oceans/sr03_98_woce/. Carbon Dioxide Information Analysis Center, Oak Ridge National Laboratory, US Department of Energy, Oak Ridge, Tennessee. (2013).

83 McNeil, B. I. & Tilbrook, B. A seasonal carbon budget for the sub-Antarctic Ocean, South of Australia. *Mar Chem* **115**, 196-210 (2009).

84 Sarmiento, J. L. *et al.* A new estimate of the $CaCO_3$ to organic carbon export ratio. *Glob. Biogeochem. Cycles* **16**, 10.1029/2002GB001919 (2002).

85 King, A. L. & Howard, W. R. Planktonic foraminiferal $\delta^{13}C$ records from Southern Ocean sediment traps: New estimates of the oceanic Suess effect. *Glob. Biogeochem. Cycles* **18**, 10.1029/2003GB002162 (2004).

86 Spero, H. J., Bijma, J., Lea, D. W. & Bemis, B. E. Effect of seawater carbonate concentration on foraminiferal carbon and oxygen isotopes. *Nature* **390**, 497-500 (1997).

87 Bemis, B. E., Spero, H. J., Lea, D. W. & Bijma, J. Temperature influence on the carbon isotopic composition of *Globigerina bulloides* and *Orbulina universa* (planktonic foraminifera). *Mar. Micropaleontol.* **38**, 213-228 (2000).

Supplementary Information: Heterogenous contribution of the Southern Ocean to deglacial atmospheric CO2 rise

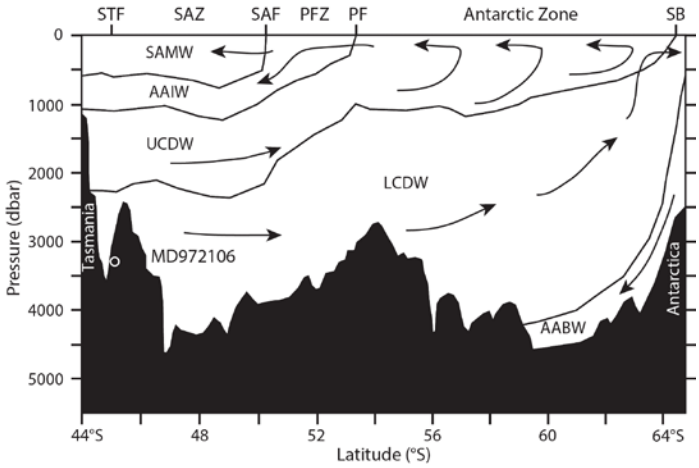

Supplementary Figure 1. Circulation and deep-water masses along WOCE SR3 line transect. MD972106 (45°09'S, 146°17'E, water depth 3310 m) is located at the southern edge of the Subtropical front and bathed in Lower Circumpolar Deep Water. STF = Subtropical Front, SAZ = Subantarctic Zone, SAF = Subantarctic Front, PFZ = Polar Frontal Zone, PF = Polar Front, SB = southern boundary of the ACC, SAMW = Subantarctic Mode Water, AAIW = Antarctic Intermediate Water, UCDW = Upper Circumpolar Deep Water, LCDW = Lower Circumpolar Deep Water and AABW = Antarctic Bottom Water. Southern Ocean frontal locations and water masses in the South Tasman Rise region are well defined through the WOCE SR3 repeat hydrographic section between Tasmania and Antarctica[1-4]. Climatological data from the World Ocean Atlas 2013 (WOA13; 0.25°)[5], shows modern summer and winter sea surface temperatures (SST) of 14.0°C and 11.0°C at MD972106, respectively, indicating that the core site is located at the southern edge of the STF. Southern Ocean frontal locations and water mass profiles compiled from Rintoul and Bullister (ref. 1) and Sokolov and Rintoul (ref. 4).

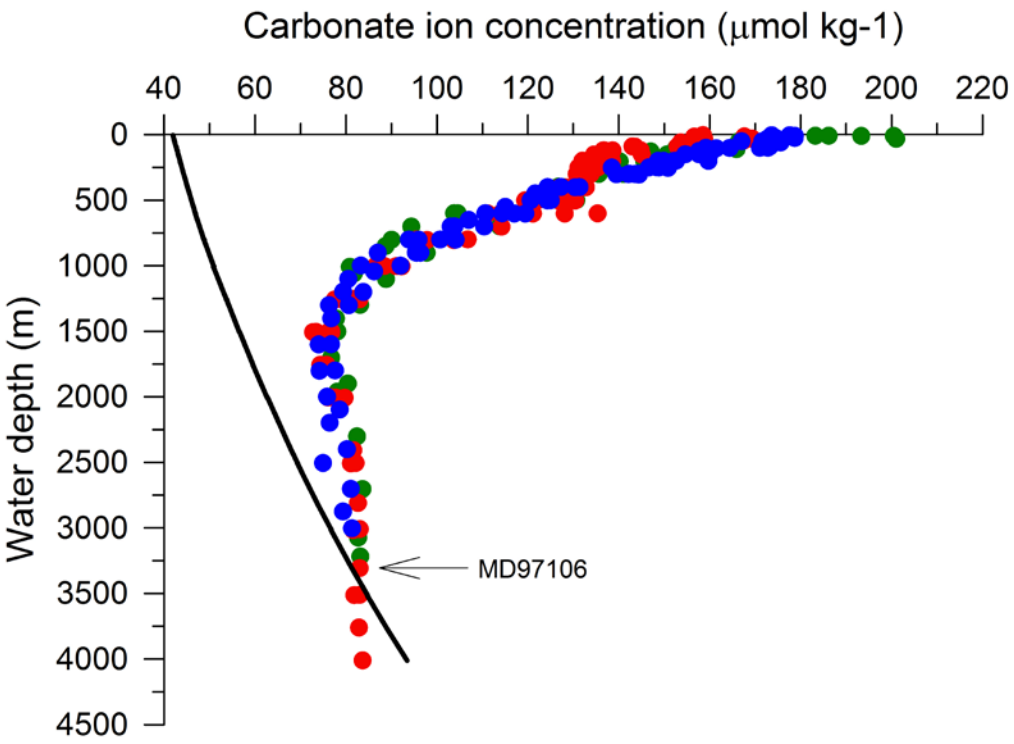

Supplementary Figure 2. WOCE line SR3 vertical profiles of carbonate ion concentration ($[CO_3^{2-}]$) between 44°S and 46°S, and calcite solubility (solid line). The seawater calcite saturation horizon occurs at ~3,500 m water depth. MD972106 (45°09'S, 146°17'E, water depth 3310 m) is located above the modern calcite saturation horizon and above the foraminiferal lysocline that occurs at ~3,600 m water depth[6]. $[CO_3^{2-}]$ are from WOCE line SR3 section from voyage AA9404 (green circles), AA0301 (blue circles) and AA9706 (red circles). $[CO_3^{2-}]$ was calculated from TA, DIC, temperature, pressure, salinity, $[PO_4^{3-}]$ and $[SiO_4^{4-}]$ from the WOCE line SR3 section between 44° S and 46° S (refs 7-9) using the CO2Sys Excel macro (version 2.1) (ref. 10) and constants from Mehrbach *et al*. (ref. 11) refitted by Dickson and Millero (ref. 12). Calcite solubility was calculated from the equation of Mucci (ref. 13) that includes pressure adjustments in K_{sp} following Ingle (ref. 14).

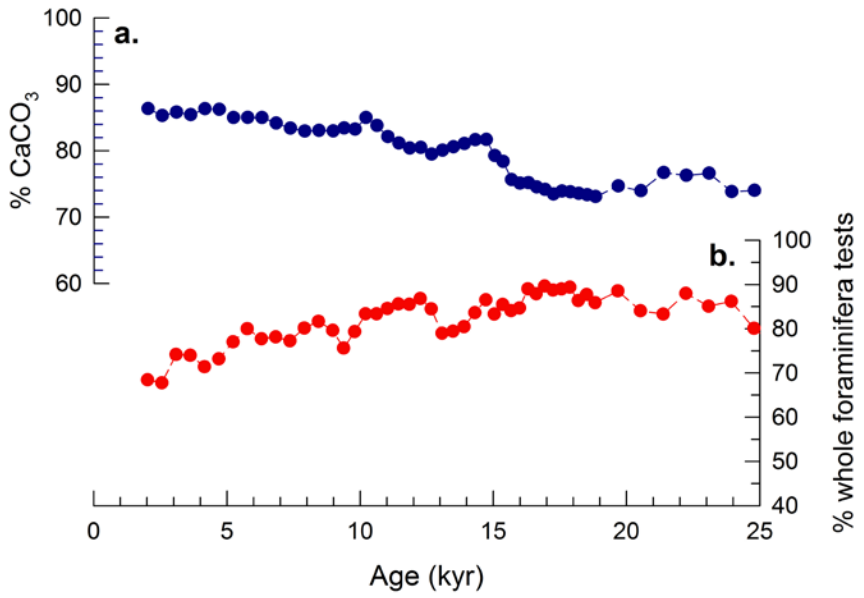

Supplementary Figure 3. Indicators of post-depositional dissolution. Carbonate Preservation Indices (%$CaCO_3$ and %whole foraminiferal tests) for MD972106, **a**, %$CaCO_3$ for MD972106 (blue circles) and **b**, %whole foraminiferal (%WF) (red circles) as a function of age (ka). The timescale for MD972106 is based on radiocarbon dates (see Methods). %$CaCO_3$ is highest during the Holocene (~85%) and decreases to ~75% during the Last Glacial Maximum (LGM). Similarly, %WF is lowest during Holocene (~76%) and increases during to ~86 % during the LGM. At MD972106 (and other South Tasman Rise sites[15]), the pattern of decreasing %$CaCO_3$ during the LGM likely results in part from the dilution of carbonate by terrigenous sediment[15]. MD972106 is located above the modern calcite saturation horizon (at ~3,500m water depth; Supplementary Fig. 2). Holocene core-top *G. bulloides* (300-355 μm) shell weights indicate the foraminiferal lysocline at the South Tasman Rise occurs at ~3,600m water depth[6]. These indicators of post-depositional dissolution suggest that dissolution did not play an important role over the past 25 kyr at MD972106. %$CaCO_3$ are from Moy *et al.*, (ref. 16) and %WF were determined using similar methods to those described by Howard and Prell (ref. 17).

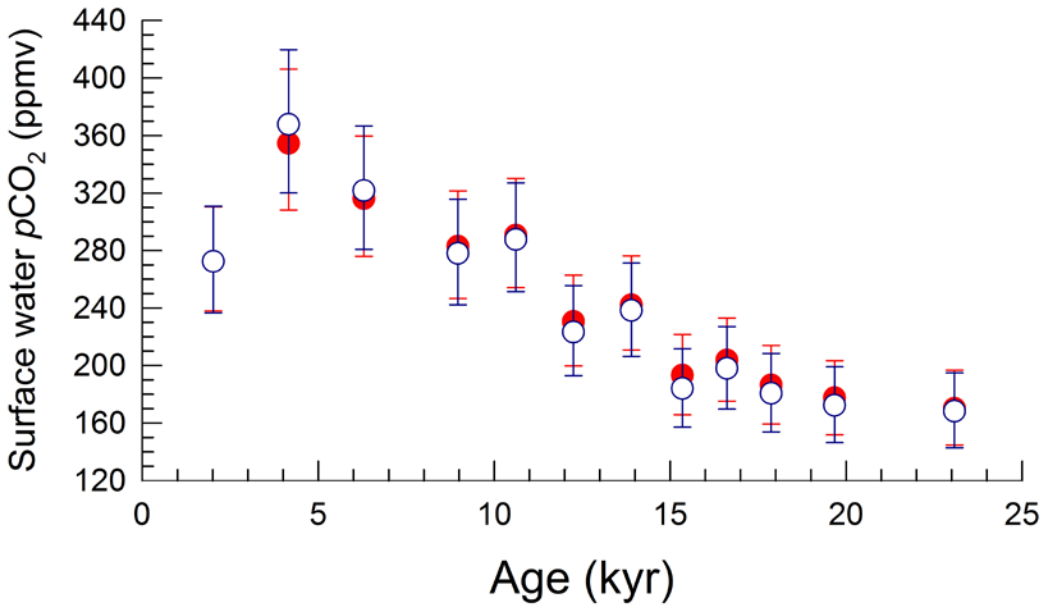

Supplementary Figure 4. Reconstructed surface water pCO_2 from pH, alkenone SST and DIC (Method 2) at the MD972106 site over the past 25,000 years. For Method 2, temperature and [CO_3^{2-}] adjustments on *G. bulloides* $\delta^{13}C$ used to estimate DIC do not significantly change the pCO_2 estimates for this method. The average difference in pCO_2 estimates calculated from (a) boron isotope-based pH estimates and DIC (where *G. bulloides* $\delta^{13}C$ is not temperature and [CO_3^{2-}]-adjusted; blue open circles) and (b) boron isotope-based pH estimates and DIC (where *G. bulloides* $\delta^{13}C$ is temperature- and [CO_3^{2-}]-adjusted; red circles) is ~2 ppm. The small average pCO_2 difference of ~2 ppm indicates that the temperature and [CO_3^{2-}] adjustments on *G. bulloides* $\delta^{13}C$ used to estimate DIC do not play a significant role in pCO_2 estimates for Method 2. *G. bulloides* $\delta^{13}C$ values were adjusted for temperature and for [CO_3^{2-}] (see Methods). Error bars represent 95% confidence intervals around the Monte Carlo mean, where 2σ uncertainties on the individual input variables and other carbonate system parameters are propagated via the Monte Carlo simulation (n = 10,000) in the statistical analysis program R (Methods).

Supplementary Note 1 Anthropogenic-influenced surface water pH, pCO_2 and [CO_3^{2-}] at the MD972106 site calculated using WOCE line SR3 data from voyage AA0301 (ref. 8; Fig. 1 in main text) and the CO2Sys Excel macro (version 2.1) (ref. 10) and constants from Mehrbach *et al*. (ref. 11) refitted by Dickson and Millero (ref. 12).

Supplementary Note 2 Anthropogenic CO_2 value for surface waters from the WOCE line SR3 close to MD972106 site are ~45 μmol kg^{-1} (GLODAP v1.1 database[18]), which corresponds to a [CO_3^{2-}] decrease of ~29 μmol kg^{-1} with respect to estimated pre-industrial values. Present-day surface [CO_3^{2-}] is ~183 μmol kg^{-1}; thus pre-industrial [CO_3^{2-}] is estimated to be ~212 μmol kg^{-1}. Calculated [CO_3^{2-}] for surface waters are from WOCE line SR3 TA, DIC, temperature, pressure, salinity, [PO_4^{3-}] and [SiO_4^{4-}] from the GLODAP v1.1 database[18] using the CO2Sys Excel macro (version 2.1) (ref. 10) and constants from Mehrbach *et al*. (ref. 11) refitted by Dickson and Millero (ref. 12).

SUPPLEMENTARY REFERENCES

1 Rintoul, S. R. & Bullister, J. L. A late winter hydrographic section from Tasmania to Antarctica. *Deep Sea Res. Part I Oceanogr. Res. Pap.* **46**, 1417-1454 (1999).

2 Rintoul, S. R., Donguy, J. R. & Roemmich, D. H. Seasonal evolution of upper ocean thermal structure between Tasmania and Antarctica. *Deep-Sea Research Part II* **44**, 1185-1202 (1997).

3 Rintoul, S. R. & Trull, T. W. Seasonal evolution of the mixed layer in the Subantarctic Zone south of Australia. *J. Geophys. Res.* **106**, 31,447-431,462 (2001).

4 Sokolov, S. & Rintoul, S. R. Structure of Southern Ocean fronts at 140°E. *J. Mar. Syst.* **37**, 151-184 (2002).

5 Locarnini, R. A. *et al. World Ocean Atlas 2013, Volume 1: Temperature. S. Levitus, Ed.; A. Mishonov, Technical Ed.*, (2013).

6 Moy, A. D., Howard, W. R., Bray, S. G. & Trull, T. W. Reduced calcification in modern Southern Ocean planktonic foraminifera. *Nat Geosci* **2**, 276-280 (2009).

7 Tilbrook, B. & Rintoul, S. Hydrographic, chemical and total CO_2 data obtained during RSV *Aurora Australis* in the Southern Pacific Ocean during WOCE section P12 (SR3/S04, EXPOCODE 09AR9404_1), (13 December, 1994 - 02 February, 1995). http://cdiac.ornl.gov/ftp/oceans/p12woce/. Carbon Dioxide Information Analysis Center, Oak Ridge National Laboratory, US Department of Energy, Oak Ridge, Tennessee. (1995).

8 Tilbrook, B., Rintoul, S. & Sabine, C. L. Carbon dioxide, hydrographic and chemical data obtained during R/V *Aurora Australis* repeat hydrography cruise in the Southern Ocean: CLIVAR CO_2 repeat section SR03_2001 (EXPOCODE AA0301), (29 October - 22 November, 2001). http://cdiac.ornl.gov/ftp/oceans/CLIVAR/SR03_AA0301_2001.data/. Carbon Dioxide Information Analysis Center, Oak Ridge National Laboratory, US Department of Energy, Oak Ridge, Tennessee. (2001).

9 Tilbrook, B., McNeil, B. & Rosenberg, M. Hydrographic, chemical and carbon data obtained during RSV *Aurora Australis* in the Southern Pacific Ocean during WOCE section SR03, (EXPOCODE 09AR19980228), (28 February - 01 April, 1988). http://cdiac.ornl.gov/ftp/oceans/sr03_98_woce/. Carbon Dioxide

Information Analysis Center, Oak Ridge National Laboratory, US Department of Energy, Oak Ridge, Tennessee. (2013).

10 Pierrot, D. E., Lewis, E. & Wallace, D. W. R. MS excel program developed for CO2SYS system calculations. ORNL/CDIAC-105a. Carbon Dioxide Information Analysis Center, Oak Ridge National Laboratory, U.S. Department of Energy, Oak Ridge, Tennessee. (2006).

11 Mehrbach, C., Culberton, C. H., Hawley, J. E. & Pytkowicz, R. M. Measurement of the apparent dissociation constants of carbonic acid in seawater at atmospheric pressure. *Limnol. Oceanogr.* **18**, 897-907 (1973).

12 Dickson, A. G. & Millero, F. J. A comparison of the equilibrium constants for the dissociation of carbonic acid in seawater media. *Deep Sea Res. Part II* **34**, 1733-1743 (1987).

13 Mucci, A. The solubility of calcite and aragonite in seawater at various salinities, temperatures and one atmosphere total pressure. *Am. J. Sci.* **283**, 780-799 (1983).

14 Ingle, S. E. Solubility of calcite in the ocean. *Mar. Chem.* **3**, 301-319 (1975).

15 Connell, R. D. & Sikes, E. L. Controls on the Late Quaternary sedimentation of the South Tasman Rise. *Aust. J. Earth Sci.* **44**, 667-675 (1997).

16 Moy, A. D., Howard, W. R. & Gagan, M. K. Late Quaternary palaeoceanography of the Circumpolar Deep Water from the South Tasman Rise. *J. Quat. Sci.* **21**, 763-777 (2006).

17 Howard, W. R. & Prell, W. L. Late Quaternary $CaCO_3$ production and preservation in the Southern Ocean: Implications for oceanic and atmospheric carbon cycling. *Paleoceanography* **9**, 453-482 (1994).

18 Key, R. M. *et al.* A global ocean carbon climatology: Results from Global Data Analysis Project (GLODAP). *Glob. Biogeochem. Cycles* **18**, 10.1029/2004GB002247 (2004).